

N72-11491

THEORETICAL CHEMISTRY INSTITUTE

THE UNIVERSITY OF WISCONSIN

**CASE FILE
COPY**

COMPUTATIONAL INVESTIGATIONS OF LOW-DISCREPANCY POINT SETS

Tony T. Warnock

WIS-TCI-453

27 August 1971

MADISON, WISCONSIN

COMPUTATIONAL INVESTIGATIONS OF LOW-DISCREPANCY POINT SETS *

by

Tony T. Warnock

Computer Sciences Department and Theoretical Chemistry Institute

University of Wisconsin

Madison, Wisconsin 53706

ABSTRACT

The quasi-Monte Carlo method of integration offers an attractive solution to the problem of evaluating integrals in a large number of dimensions; however, the associated error bounds are difficult to obtain theoretically. Since these bounds are associated with the L^2 discrepancy of the set of points used in the integration, this paper presents numerical calculations of the L^2 discrepancy for several types of quasi-Monte Carlo formulae.

* This work received financial support from National Science Foundation Grant GB-16665 and National Aeronautics and Space Administration Grant NGL 50-002-001.

The quasi-Monte Carlo method of evaluation of a multiple integral consists of averaging function values over a well-distributed set of points in the region of integration. This method differs from classical methods in which a part of some representation (polynomial, Fourier series) of the function is integrated exactly, and from the ordinary Monte Carlo method where a "random" sample of function values is averaged. Error bounds for quasi-Monte Carlo integration can be based on various measures of the inequity in the distribution of the set of points over which the function is averaged. Any integration formula may be treated as quasi-Monte Carlo by using the bounds discussed below.

This paper gives the results of some computational studies of the L^2 discrepancy of several types of sets of points which have been suggested as being suitable for quasi-Monte Carlo integration of functions in the unit K -cube.

The local discrepancy, $g(\underline{\xi})$, at a point $\underline{\xi}$ in the unit K -cube ($0 < \xi_i \leq 1, i = 1, \dots, K$), of a set of points $\underline{X} = \{\underline{x}_m\}$, $m = 1, \dots, N$, is defined by

$$g(\underline{\xi}) = N^{-1}v(\underline{\xi}) - \prod_{i=1}^K \xi_i \quad (1)$$

where $v(\underline{\xi})$ is the number of points of \underline{X} whose coordinates satisfy: $0 < x_{mi} \leq \xi_i$, [1], [2]. The function $g(\underline{\xi})$ is a measure of the local unevenness in the distribution of the points of \underline{X} . Figure 1 illustrates $g(\underline{\xi})$ in two dimensions.

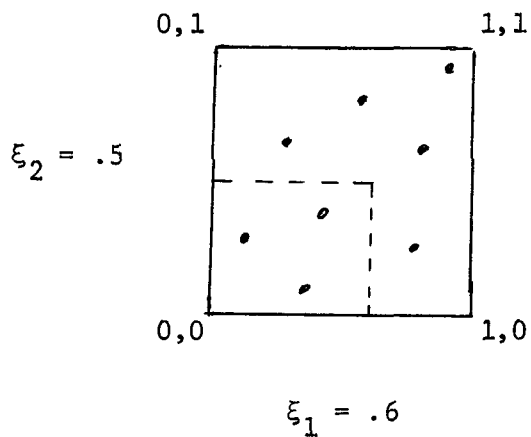


Figure 1

$$N = 8, \quad v(.6, .5) = 3$$

$$g(.6, .5) = 3/8 - .6 \times .5 = .075$$

Various norms of $g(\xi)$ taken over the unit K -cube give a global measure of unevenness and may be used to express error bounds for quasi-Monte Carlo integration, [1], [2], [3], [4].

The error, ϵ , for quasi-Monte Carlo integration is given by

$$\epsilon = \left| N^{-1} \sum_{m=1}^N f(x_m) - \int_0^1 \dots \int_0^1 f(\xi) d\xi_1 \dots d\xi_K \right|. \quad (2)$$

Although the function $g(\xi)$ is not differentiable, it can be treated as a generalized function so that the following derivation of the error bounds is correct, [1], [5]. The same result has been obtained in a different manner by Zaremba in [3]. The proof is given below for the case of two dimensions but the same argument generalizes to more dimensions without any essential change. Equation (2) can be written in the case of two dimensions

$$\epsilon = \left| \int_0^1 \int_0^1 f(\xi_1, \xi_2) - \frac{\partial^2 g(\xi_1, \xi_2)}{\partial \xi_1 \partial \xi_2} d\xi_1 d\xi_2 \right| \quad (3)$$

where the derivatives of $g(\xi)$ are generalized derivatives, [5]. Integration of (3) by parts gives

$$\epsilon = \left| \int_0^1 \int_0^1 \frac{\partial^2 f(\xi_1, \xi_2)}{\partial \xi_1 \partial \xi_2} g(\xi_1, \xi_2) d\xi_1 d\xi_2 - \int_0^1 \frac{\partial f(1, \xi_2)}{\partial \xi_2} g(1, \xi_2) d\xi_2 - \int_0^1 \frac{\partial f(\xi_1, 1)}{\partial \xi_1} g(\xi_1, 1) d\xi_1 \right| \quad (4)$$

since the other terms from the integration by parts vanish identically, [3]. Application of the triangle inequality to (4) gives

$$\epsilon \leq \left| \int_0^1 \int_0^1 \frac{\partial^2 f(\xi_1, \xi_2)}{\partial \xi_1 \partial \xi_2} g(\xi_1, \xi_2) d\xi_1 d\xi_2 \right| + \left| \int_0^1 \frac{\partial f(1, \xi_2)}{\partial \xi_2} g(1, \xi_2) d\xi_2 \right| + \left| \int_0^1 \frac{\partial f(\xi_1, 1)}{\partial \xi_1} g(\xi_1, 1) d\xi_1 \right|, \quad (5)$$

From the definition of $g(\xi)$, it can be seen that $g(1, \xi_2)$ and $g(\xi_1, 1)$ are the local discrepancies of the points $\tilde{X} = \{x_{m1}, x_{m2}\}$ projected onto the ξ_2 and ξ_1 axes respectively.

Of the possible bounds obtainable from (5), the one discussed here comes from an application of the Cauchy-Schwarz inequality to (5), [3]. The L^2 norm of $g(\xi)$, denoted by $T(\tilde{X})$, (the L^2 or meansquare discrepancy of \tilde{X}) is defined by

$$T(\tilde{X}) = \left\{ \int_0^1 \dots \int_0^1 [g(\xi)]^2 d\xi_1 \dots d\xi_K \right\}^{1/2}, \quad (6)$$

Combining (6) with (5) using the Cauchy-Schwarz inequality gives the bound, in two dimensions,

$$\varepsilon \leq \left\{ \int_0^1 \int_0^1 \left[\frac{\partial^2 f(\xi_1, \xi_2)}{\partial \xi_1 \partial \xi_2} \right]^2 d\xi_1 d\xi_2 \right\}^{1/2} T(X) + \left\{ \int_0^1 \left[\frac{\partial f(\xi, 1)}{\partial \xi_1} \right]^2 d\xi_1 \right\}^{1/2} T_1(X) + \left\{ \int_0^1 \left[\frac{\partial f(1, \xi_2)}{\partial \xi_2} \right]^2 d\xi_2 \right\}^{1/2} T_2(X) \quad (7)$$

In (7), $T_1(X)$ and $T_2(X)$ are the L^2 discrepancies of the projections of X onto the ξ_1 and ξ_2 axes.

It is possible to obtain bounds on ε in terms of the extreme discrepancy, $D(X) = \sup_{0 \leq \xi \leq 1} g(\xi)$, and the total variation in the sense of Hardy and Krause of $f(\xi)$, [1], [3], [6]. Because $T(X)$ is much easier to compute than $D(X)$, this paper will deal with $T(X)$ only.

In Equation (7) the partial derivatives with some $\xi_i = 1$ may be replaced by those with that $\xi_i = 0$ by making the change of variable $\xi'_i = 1 - \xi_i$. Since $\int_0^1 f(\xi_i) d\xi_i = \int_0^1 f(\xi'_i) d\xi'_i$ and $\frac{\partial f(\xi'_i)}{\partial \xi'_i} = - \frac{\partial f(\xi_i)}{\partial \xi_i}$,

Equation (7) is valid as only the squares of the partial derivatives are used.

In order to utilize the bounds, (7), in numerical calculations, it is necessary to have some idea of the behavior of $T(X)$ as a function of N . A few theoretical results are available. Roth has shown that $T(X) \geq C_K N^{-1} (\ln N)^{\frac{K-1}{2}}$ for any set of N points X in K dimensions; the C_K are independent of N , [9]. Sequences have been suggested for which $T(X) \leq B_K N^{-1} (\ln N)^{K-1}$ where the B_K depend only on K [10]. One sequence has been constructed in two dimensions with $T(X) \sim AN^{-1} (\ln N)^{1/2}$ with A a constant [2]. The theoretical behavior of $T(X)$ for a random sequence is $T(X) = [(1/2)^K - (1/3)^K]^{1/2} N^{-1/2}$, [1]. In view of the difficulty

of obtaining theoretical values for $T(\tilde{X})$, this paper gives the results of computations of $T(\tilde{X})$ for various sequences which have been suggested in the literature. Also discussed are some new sequences based on computational experience.

For purposes of computation, it is more convenient to work with the expression for $N^2 T^2(\tilde{X})$, denoted by $J(\tilde{X})$. Formulae for efficient computation of $J(\tilde{X})$ in terms of the coordinate values of \tilde{X} are given below, [7], [2]. By using the Heaviside function $H(z) = 1$ for $z > 0$ and $H(z) = 0$ for $z < 0$, $g(\xi)$ can be written as

$$g(\tilde{\xi}) = N^{-1} \sum_{m=1}^N \prod_{i=1}^K H(\xi_i - x_{mi}) - \prod_{i=1}^K \xi_i. \quad (8)$$

Now $J(\tilde{X})$ becomes

$$J(\tilde{X}) = \int_0^1 \dots \int_0^1 \left[\sum_{m=1}^N \sum_{n=1}^N \prod_{i=1}^K H(\xi_i - x_{mi}) H(\xi_i - x_{ni}) - 2N \sum_{m=1}^N \prod_{i=1}^K \xi_i H(\xi_i - x_{ni}) + N^2 \prod_{i=1}^K \xi_i^2 \right] d\xi_1 \dots d\xi_K. \quad (9)$$

Since each factor in each term of the integrand depends upon only one integration variable ξ_i , the integration of each factor may be carried out separately to yield

$$J(\tilde{X}) = \sum_{m=1}^N \sum_{n=1}^N \prod_{i=1}^K [1 - \max(x_{mi}, x_{ni})] - 2^{-K+1} N \sum_{m=1}^N \prod_{i=1}^K (1 - x_{ni}^2) + 3^{-K} N^2. \quad (10)$$

For faster computation (10) may be written as

$$\begin{aligned}
 J(\underline{X}) = & \frac{1}{2} \sum_{m=1}^N \sum_{n=1}^N \prod_{i=1}^K [1 - \max(x_{mi}, x_{ni})] + \sum_{m=1}^N \prod_{i=1}^K (1 - x_{mi}) - 2N^{-K+1} \sum_{m=1}^N \prod_{i=1}^K (1 - x_{ni}^2) \\
 & + 3^{-K} N^2
 \end{aligned} \tag{11}$$

The time required for evaluation of $J(\underline{X})$ using (11) is roughly proportional to N^2 . For a sequence such as the Halton sequence, [3], it is more efficient to compute $J(\underline{X})$ for N points from that for $N-1$ points. Equations (12a - 12e) outline this calculation.

$$(12a) \quad J(\underline{X}) = P(N) - 2^{-K+1} N Q(N) + 3^{-K} N^2$$

$$(12b) \quad P(1) = \prod_{i=1}^K (1 - x_{1i})$$

$$(12c) \quad Q(1) = \prod_{i=1}^K (1 - x_{1i}^2)$$

$$(12d) \quad P(N) = P(N-1) + 2 \sum_{m=1}^{N-1} \prod_{i=1}^K [1 - \max(x_{mi}, x_{Ni})] + \prod_{i=1}^K (1 - x_{Ni})$$

$$(12e) \quad Q(N) = Q(N-1) + \prod_{i=1}^K (1 - x_{Ni}^2)$$

These equations the computation of $J(\underline{X})$ in a time roughly proportional to N^2 for each set of M points from $M = 1, \dots, N$, where each successive point is added to the previous set without altering the coordinates of the previous points. A somewhat more elaborate set of formulae (13a - 13i) may be used to achieve a similar savings in time for a sequence such as

Hammersley's, [3], where the first coordinate is always equally spaced at intervals of $1/N$.

$$(13a) \quad \tilde{T}(X) = P(N) - N^{-1} \hat{P}(N) - 2^{-K+1} NQ(N) + 2^{-K+1} N^{-2} Q(N) + 3^{-K} N^2$$

$$(13b) \quad P(1) = \hat{P}(1) = \prod_{i=2}^K (1 - x_{1i})$$

$$(13c) \quad Q(1) = \hat{Q}(1) = \prod_{i=2}^K (1 - x_{1i}^2)$$

$$(13d) \quad \Delta P = 2 \sum_{m=1}^{N-1} \prod_{i=2}^K [1 - \max(x_{mi}, x_{Ni})] + \prod_{i=2}^K (1 - x_{Ni})$$

$$(13e) \quad \Delta Q = \prod_{i=2}^K (1 - x_{Ni}^2)$$

$$(13f) \quad P(N) = P(N-1) + \Delta P$$

$$(13g) \quad \hat{P}(N) = \hat{P}(N-1) + N\Delta P$$

$$(13h) \quad Q(N) = Q(N-1) + \Delta Q$$

$$(13i) \quad \hat{Q}(N) = \hat{Q}(N-1) + N^2 \Delta Q$$

Figures 2 through 9 are plots of $\tilde{T}(X)$ vs. N for several sequences in 2 through 9 dimensions. The values of $\tilde{T}(X)$ are plotted for N running from 25 to 1000 in steps of 25, except for the good lattice sequences where N is not necessarily a multiple of 25 and the sequences which were derived by computation where all values of N were not tried. Figure 10 is an extension of Figure 9 to 2000 points only sequences 2, 6, and 7 are plotted. Sequence 4 is slightly below Sequence 2 but not

enough to show on the graph. Figure 11 is an expanded version of Figure 4 showing $T(\tilde{X})$ at each N for N running from 150 to 190. The solid line represents $T(\tilde{X})$ for a canonical random sequence. All the points are not plotted since otherwise the graphs would become rather crowded.

Each sequence described below consists of sets of N points \tilde{x}_m where $m = 0, \dots, N - 1$. The first point \tilde{x}_0 is placed at $(1, 1, \dots)$ instead of $(0, 0, \dots)$ as is usual because computational experience suggests that this will give a lower value of $T(\tilde{X})$ in general.

Sequence 1, \square on the graphs, is the Halton sequence [3], defined in K dimensions by $\tilde{x}_m = (\phi_2(m), \phi_3(m), \dots, \phi_{P_K}(m))$ where the P 's are the first K primes. The function $\phi_r(m)$ is the radical-inverse function of m to the base r . If an integer $m = a_0 + a_1r + a_2r^2 + \dots$, where the a_i are uniquely defined integers in $\{0, 1, \dots, r-1\}$ for any integer radix $r \geq 2$, then $\phi_r(m) = a_0r^{-1} + a_1r^{-2} \dots$. The function is equivalent to taking the r -ary representation of the number m and reflecting the digits about the radical point. For example $10 = 1010_2$ (numbers without subscript are base ten) so $\phi_2(10) = 0.101_2$ or $5/16$; and $11 = 102_3$ so $\phi_3(11) = .201_3 = 19/27$.

Sequence 2, \circ , is the Hammersley sequence defined by $\tilde{x}_m = (m/N, \phi_2(m), \dots, \phi_{P_{K-1}}(m))$, [3].

Sequence 3, \blacksquare , is a modified generalization of a idea due to Zaremba, [2]. The function $\psi_r(m)$, the folded radical inverse function, is defined similarly to $\phi_r(m)$. If the representation of m base r is $m = a_0 + a_1r + a_2r^2 + \dots$ then $\psi_r(m) = (a_0 + 0)_{\text{mod } r} r^{-1} + (a_1 + 1)_{\text{mod } r} r^{-2} + (a_2 + 1)_{\text{mod } r} r^{-3} + \dots$. The ψ_r differ from

the ϕ_r in that each coefficient a_i has its index, i , added to modules r in the expansion of ψ . For example $\psi_2(10) = .0000\overline{01}_2$ or $1/48$ and $\psi_3(11) = .2100\overline{12}_3$ or $551/702$, the [superscribed] line represents an infinitely repeated sequence of digits. The sequence is

$\tilde{x}_m = (\psi_2(m), \dots, \psi_{P_K}(m))$ which is analogous to the Halton sequence.

Sequence 4, \bullet , is the sequence $\tilde{x}_m = (m/N, \psi_2(m), \dots, \psi_{P_{K-1}}(m))$ which is analogous to the Hammersley sequence.

Sequence 5, \triangle , is the sequence $\tilde{x}_m = (\left\{ \frac{m(m+1)}{2} \sqrt{2} \right\}, \dots, \left\{ \frac{m(m+1)}{2} \sqrt{P_K} \right\})$ where $\{\alpha\}$ denotes the fractional part of α . This sequence has been suggested by Haber as a pseudo-random sequence [11].

Sequence 6, \blacktriangle , is the sequence $\tilde{x}_m = (\left\{ m\sqrt{2} \right\}, \dots, \left\{ m\sqrt{P_K} \right\})$.

Sequence 7, \blacktriangledown , is constructed from the Univac 1108 pseudo-random number generator at the University of Wisconsin. The generator is a mixed-congruential type $u_\ell = (5^{15} u_{\ell-1} + 1)_{\text{mod } 2^{35}}$, [12]. The u_ℓ are supposed to be uniformly distributed integers on the interval $(0, 2^{35}-1)$ so that $v_\ell = u_\ell / 2^{35}$ will be distributed uniformly on $(0, 1)$.

The sequence is $\tilde{x}_m = (v(m-1)K+1, v(m-1)K+2, \dots, v(m-K))$. The initial $u_0 = 5^{13}$.

The sets of points in Figures 2, 3, and 4 denoted by z are the good lattice points of Zaremba. The two dimensional sequence is described in [13] and is the sequence $\tilde{x}_m = \left(\frac{m}{F_\ell}, \left\{ \frac{mF_\ell-1}{F_\ell} \right\} \right)$ where F_ℓ is the ℓ th Fibonacci number. The lattices used in three and four dimensions were obtained computationally [14].

The sets of points in Figures 2 and 3 denoted by $+$ were computed from Sequence 4 by iteratively applying the following formula:

$$x_{pq} = [2^{-K+2} \prod_{\substack{i=1 \\ i \neq q}}^K (1 - x_{pi}^2)]^{-1} \cdot 2 \sum_{m=1}^N H(x_{pq} - x_{mq}) \prod_{\substack{i=1 \\ i \neq q}}^K [1 - \max(x_{pi}, x_{mi})] \\ + \prod_{\substack{i=1 \\ i \neq q}}^K (1 - x_{pi})$$

This formula is obtained by considering $J(\tilde{X})$ to be a function of the variable x_{pq} only. Then $J(\tilde{X})$ is a parabola in x_{pq} and the formula gives the minimum of this parabola. The computation takes a time roughly proportional to N^2 to process a set of N points.

An inspection of the graphs shows that in two through seven dimensions the sequences based on the various radical inverse functions, Sequences 1, 2, 3, 4, are better than those of the pseudo-random number generator or those based on the square roots of primes. In eight dimensions the two radical inverse sequences with equally spaced first dimension do better than the others but the two with radical inverse functions only do not do so well, at least to 1000 points. In nine dimensions the radical inverse sequences do not do so well as the other three sequences up to about 1500 points. However as the number of points is increased, these sequences perform better than either the pseudo-random generator or those based on roots of primes.

Behavior of this sort is not unexpected. The radical inverse sequences in 9 dimensions use $\phi_{19}(m)$ and $\phi_{23}(m)$ which are strongly correlated until m becomes large. As one goes to higher dimensions this behavior is intensified such that the radical inverse sequences will start decreasing

slowly but not level out so fast as the other sequences do. Figure 11 shows that all these sequences have much "fine structure" so that detailed theoretical results will be very difficult to obtain. The monotone decrease with N of sequences 2 and 4 is surprising in view of the erratic behavior of the other sequences. Although the "good lattice" points of Zaremba were constructed for integration of periodic functions, they too have low discrepancies.

The sets of points, $+ ,$ which were computed from Sequence 4 are the best so far obtained for N larger than about 100. Direct minimization of $J(\underline{X})$ is a difficult and costly procedure. Without more theoretical knowledge about the behavior of $J(\underline{X})$ as a function of the coordinate values of \underline{X} , it seems that the direct approach will not yield significant results on a large scale, but it can be used to refine any set of point to give a slightly better one.

In comparing one sequence to another, it is not so much the vertical difference in $T(\underline{X})$ at a given N that is important, but the number of points required to give a given $T(\underline{X})$. For example in 3 dimensions, to achieve the same $T(\underline{X})$ as Sequence 4 has at 200 points, Sequence 2 needs 237 points, but to equal Sequence 4 at 800 points, Sequence 2 requires 988 points. The difference in $T(\underline{X})$ is less around 700 points than around 200 points, but it takes more points Sequence 2 to make it up.

All the sequences studied here have as good or better behavior as a theoretical random sequence. Perhaps the low discrepancy of the pseudo-random number generator in several dimensions explains why computations

based on such a generator yield good results even though there may be no justification for the probabilistic bounds usually employed.

ACKNOWLEDGEMENT

The author wishes to acknowledge helpful discussions with Professor J. H. Halton.

REFERENCES

1. J. H. Halton, A Retrospective and Prospective Survey of the Monte Carlo Method, SIAM Review, 12, p. 1-63 (1970).
2. J. H. Halton and S. K. Zaremba, The Extreme and L^2 Discrepancies of Some Plane Sets, Monatsh. Math. 73, p. 316-328 (1969).
3. S. K. Zaremba, Some Applications of Multidimensional Integration by Parts, Ann. Polon. Math. 21, p. 85-96 (1968).
4. S. K. Zaremba, The Mathematical Basis of Monte Carlo and Quasi-Monte Carlo Methods, SIAM Review, 10, p. 303-314 (1968).
5. I. M. Gel'Fand and G. E. Shilou, Generalized Functions, Academic Press, New York, 1964.
6. J. F. Koksma, A General Theorem From the Theory of Uniform Distribution Modulo 1, Mathematica Zutphen, B11, p. 7-11 (1942) (Dutch).
7. E. Hlawka, Functions of Bounded Variation in the Theory of Uniform Distribution, Ann. Math. Pura. Appl. IV: 54, p. 325-334 (1961) (German).
8. K. F. Roth, On Irregularities of Distribution, Mathematica, 1, p. 73-79 (1954).
9. J. H. Halton, On the Efficiency of Certain Quasi-Random Sequences of Points in Evaluating Multidimensional Integrals, Numer. Math. 2, p. 84-90 (1960).
10. S. Haber, Numerical Evaluation of Multiple Integrals, SIAM Review, 12, 4, p. 481-526 (1970).
11. R. R. Coveyou and R. D. MacPherson, Fourier Analyses of Random Number Generators, JACM, 14, p. 100-119 (1967).

12. S. K. Zaremba, Good Lattice Points, Discrepancy, and Numerical Integration, Ann. Mat. Pura. Appl. IV: 73, p. 293-317 (1966).
13. S. K. Zaremba, Private communication.

FIGURE LEGENDS

FIGURE 2. $T(\tilde{X})$ vs. N to 1000 points in 2 dimensions.

FIGURE 3. $T(\tilde{X})$ vs. N to 1000 points in 3 dimensions.

FIGURE 4. $T(\tilde{X})$ vs. N to 1000 points in 4 dimensions.

FIGURE 5. $T(\tilde{X})$ vs. N to 1000 points in 5 dimensions.

FIGURE 6. $T(\tilde{X})$ vs. N to 1000 points in 6 dimensions.

FIGURE 7. $T(\tilde{X})$ vs. N to 1000 points in 7 dimensions.

FIGURE 8. $T(\tilde{X})$ vs. N to 1000 points in 8 dimensions.

Note vertical scale change at 500 points.

FIGURE 9. $T(\tilde{X})$ vs. N to 1000 points in 9 dimensions.

Note vertical scale change at 200 points.

FIGURE 10. Sequences 2, 6, and 7 extended from 1000 to 2000 points.

FIGURE 11. $T(\tilde{X})$ vs. N from 150 to 190 points in 4 dimensions.

Figure 2

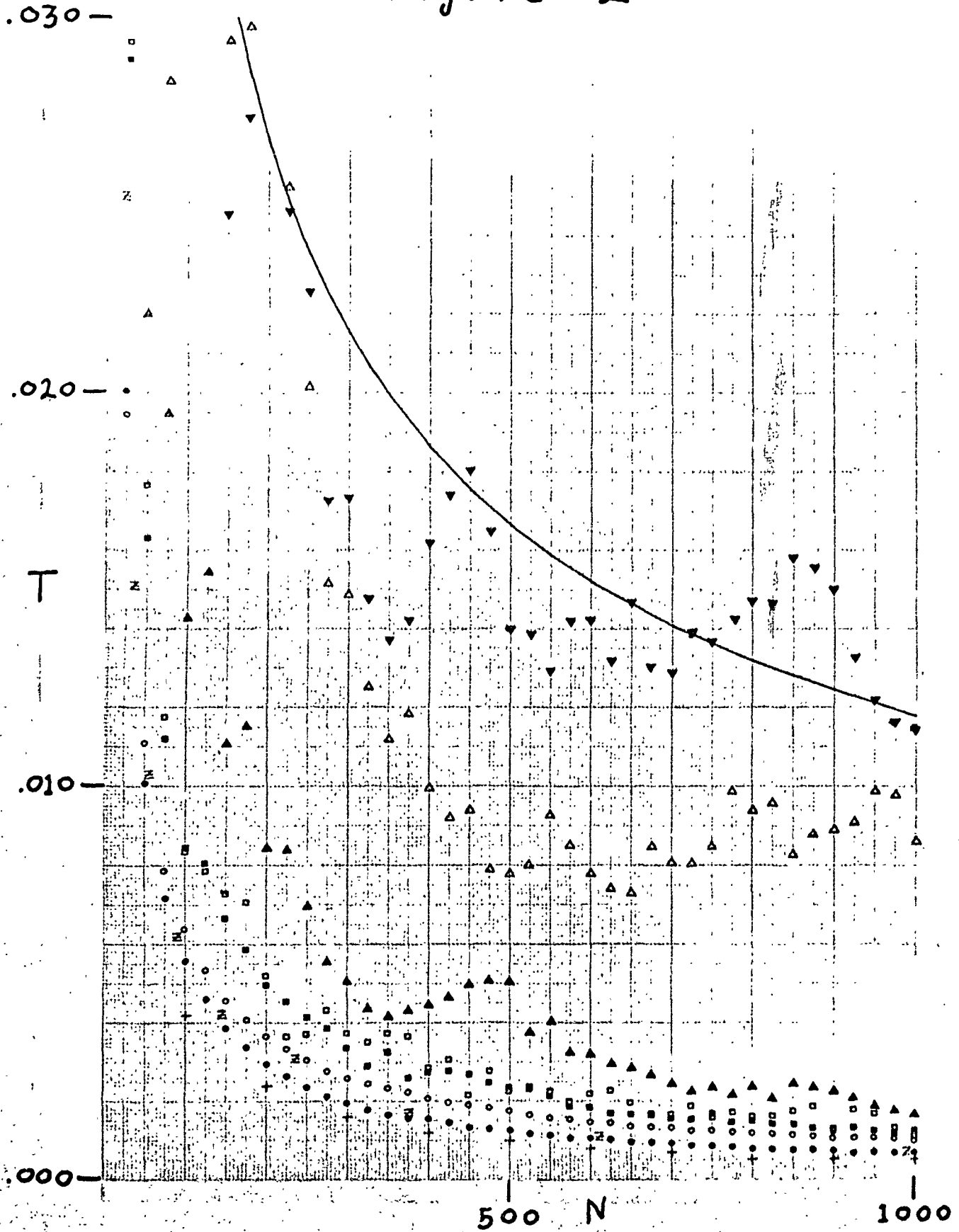


Figure 3

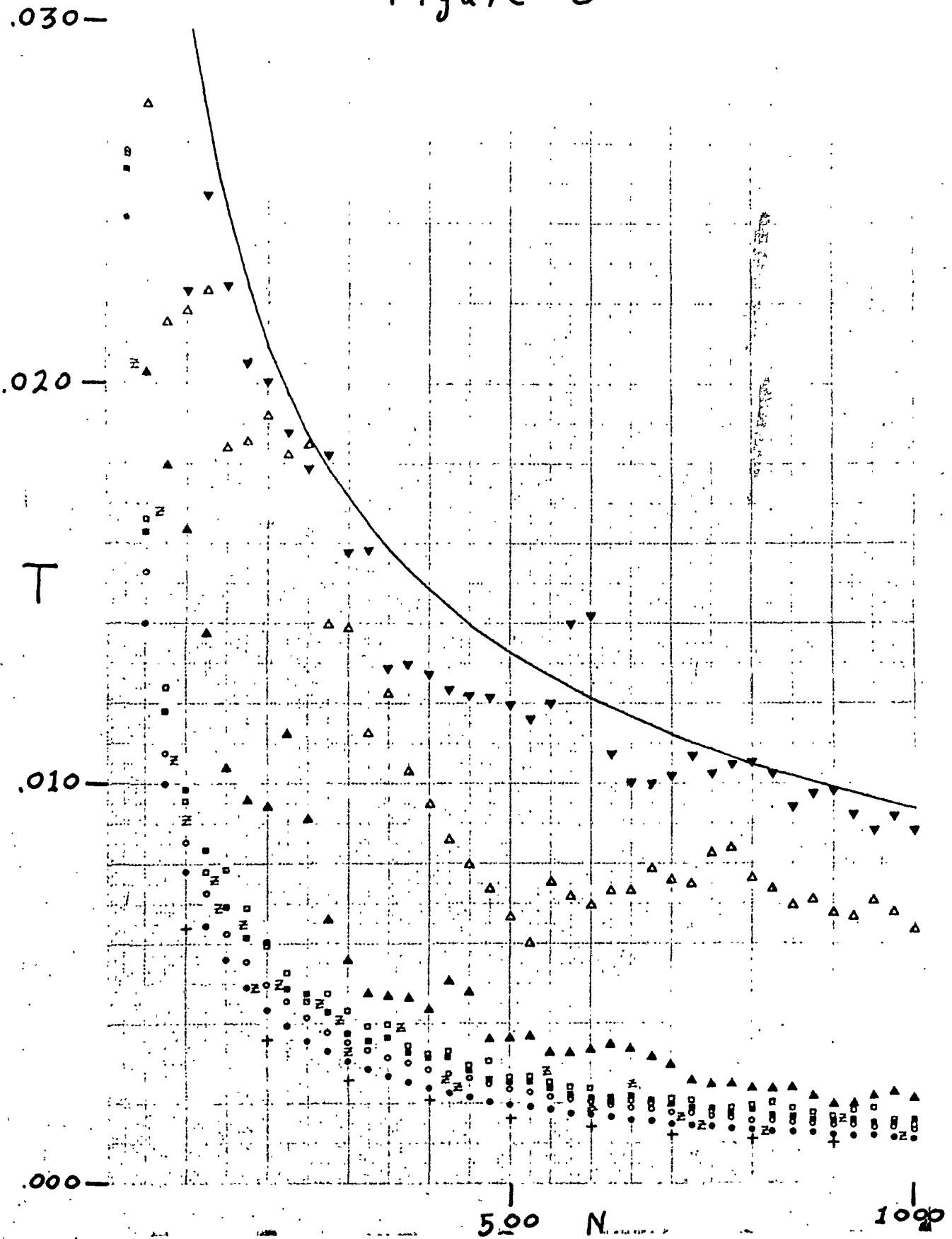


Figure 4

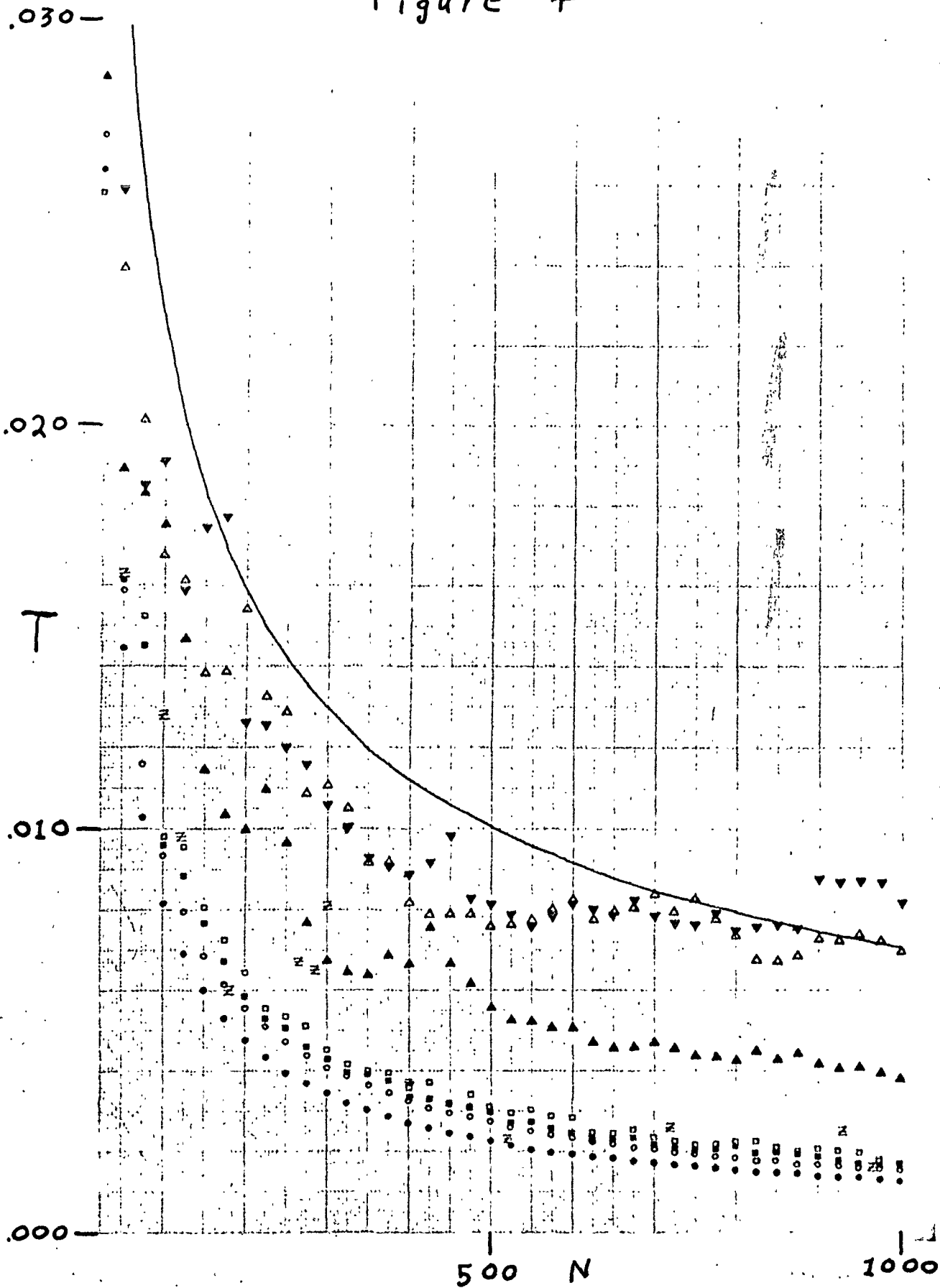


Figure 5

.030 -

.020 -

.010 -

.000 -

T

500 N

1000

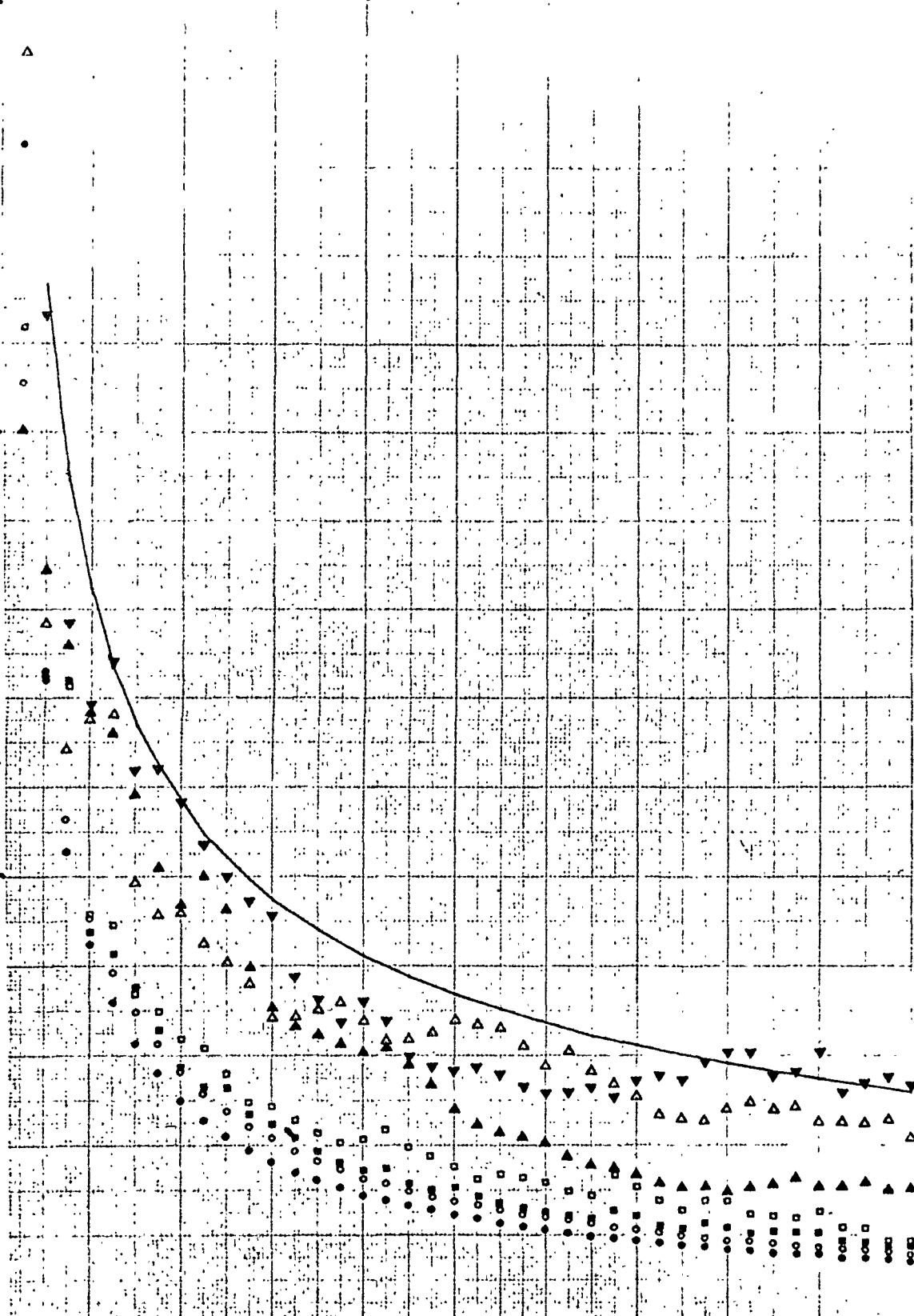


Figure 6

.030 -

.020 -

T

.010 -

.000 -

500 N

1000

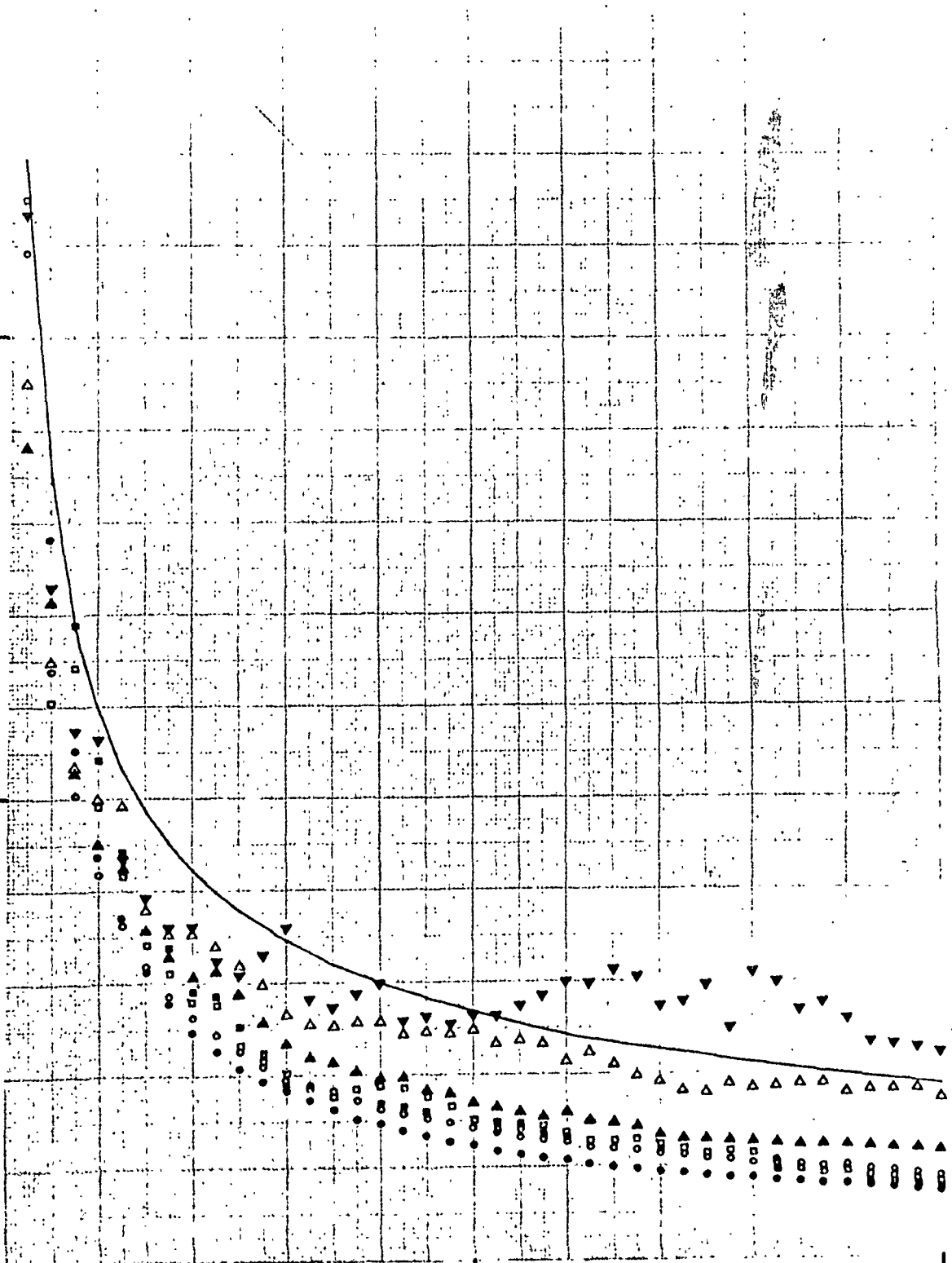


Figure 7

.030-

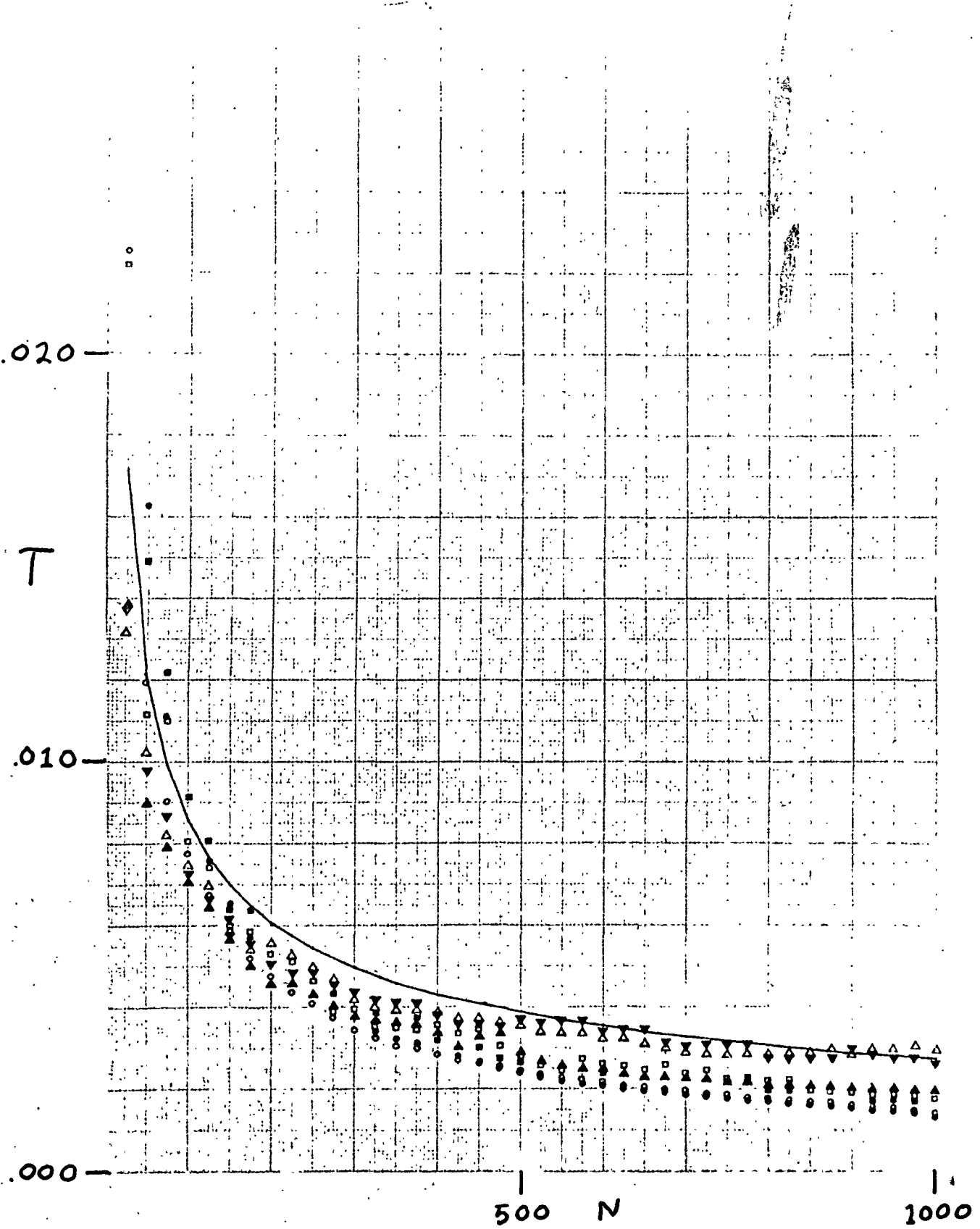
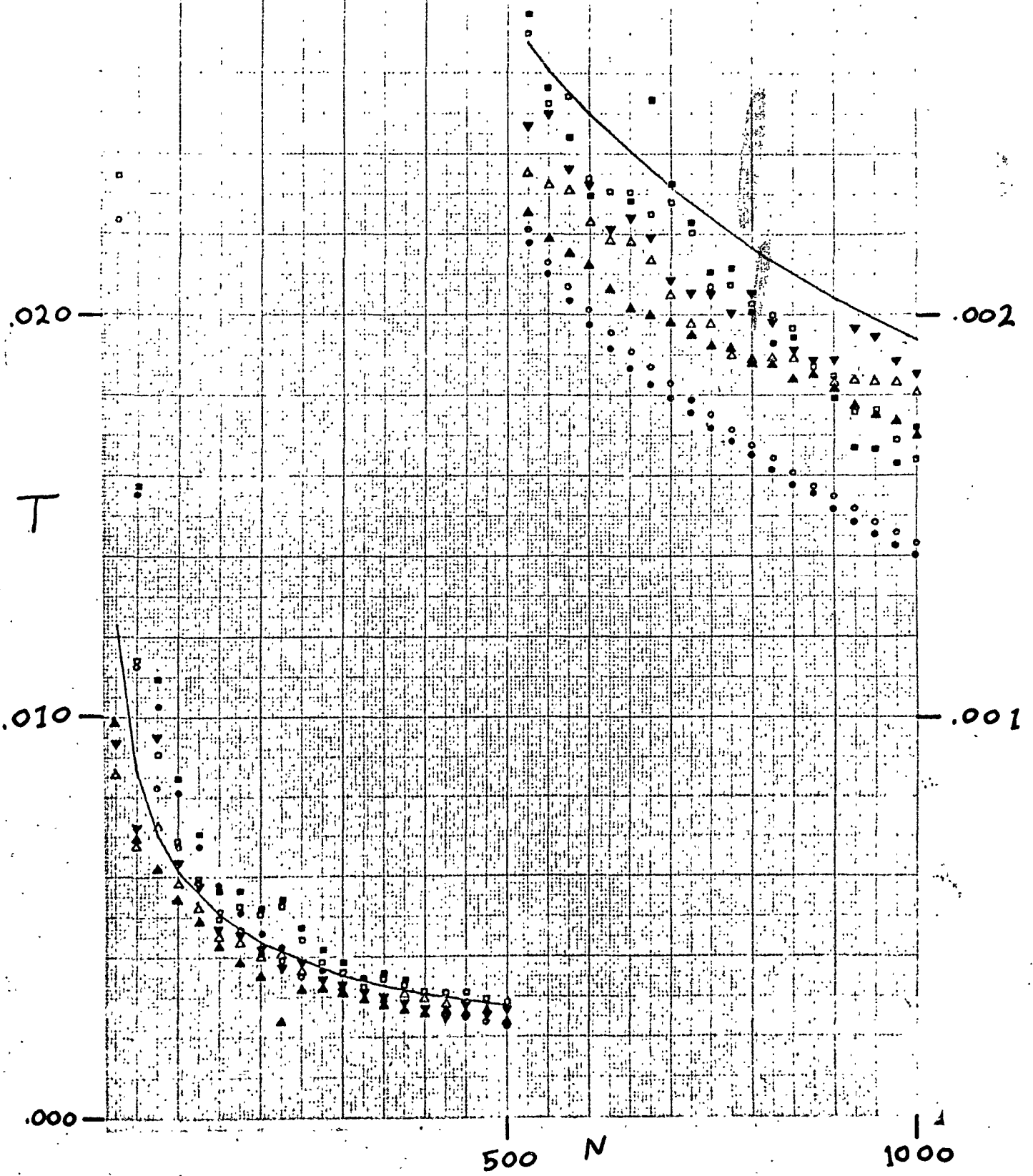


Figure 8

.030 -

- .003



.020 -

- .002

T

.010 -

- .001

.000 -

500 N

1000

Figure 9

.030-

T .003

.020-

-.002

T

.010-

-.001

.000-

500 N

1000

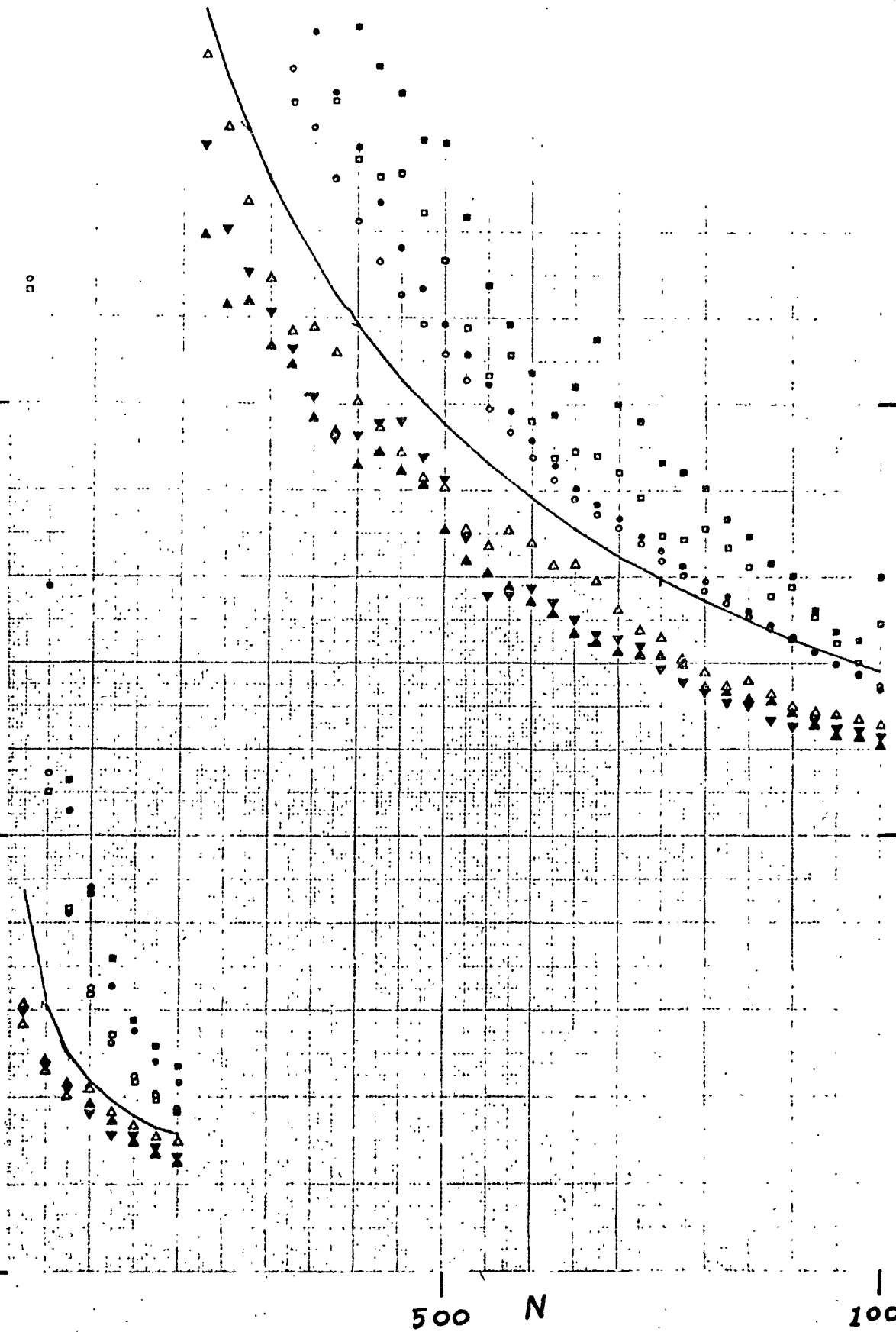
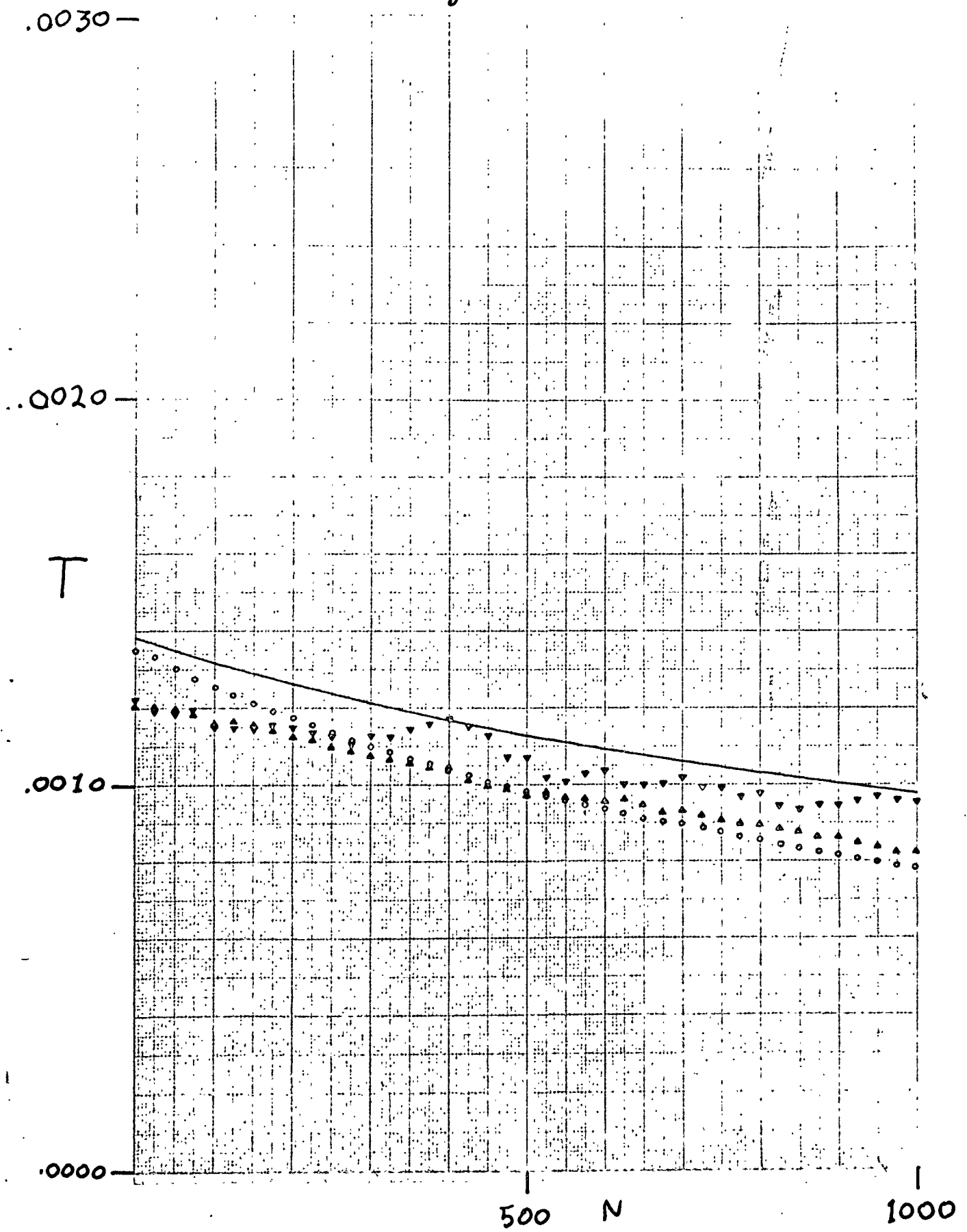


Figure 10



.030-

Figure 11

.020-

T

.010-

.000-

170

N

190

